# Brain Image Motion Correction: Impact of Incorrect Calibration and Noisy Tracking

Rasmus R. Jensen(✉), Claus Benjaminsen, Rasmus Larsen, and Oline V. Olesen

DTU Compute, Technical University of Denmark, Richard Petersens Plads, Building 321, DK-2800 Kgs. Lyngby, Denmark
{raje,clabe,rlar,ovol}@dtu.dk
http://www.compute.dtu.dk

**Abstract.** The application of motion tracking is wide, including: industrial production lines, motion interaction in gaming, computer-aided surgery and motion correction in medical brain imaging. Several devices for motion tracking exist using a variety of different methodologies. In order to use such devices a geometric calibration with the coordinate system in which the motion has to be used is often required. While most devices report a measuring accuracy and precision, reporting a calibration accuracy is not always straight forward. We set out to do a quantitative measure of the impact of both calibration offset and tracking noise in medical brain imaging. The data are generated from a phantom mounted on a rotary stage and have been collected using a Siemens High Resolution Research Tomograph for positron emission tomography. During acquisition the phantom was tracked with our latest tracking prototype. The combined data set form a good basis for a quantitative analysis of calibration accuracy and tracking precision on motion corrected medical images and scanner resolution.

**Keywords:** Motion correction · Motion tracking · Calibration · PET · Medical imaging

## 1 Introduction

Motion tracking is used in a wide range of settings. Examples are found in industrial production lines [4], gaming with user-motion interaction, computer-aided surgery [6,21] and motion correction in medical brain imaging [1,7,12,13,17,19]. The tracked motions are often obtained using secondary devices and multiple solutions exist. These solutions are based on a variety of methodologies e.g. optical systems [11,21], magnetic spatial measurement systems [6,18,20], radio-frequency [5,17], videometric systems with one or multiple cameras [1,3,12,19], accelerometers and gyroscopes [9], and structured light systems [8,13]. The tracking device has to be geometrically calibrated with the unit that uses the information for motion control or motion compensation. The tracked motion has to be transformed into the application coordinate system such as that of

© Springer International Publishing Switzerland 2015
R.R. Paulsen and K.S. Pedersen (Eds.): SCIA 2015, LNCS 9127, pp. 152–161, 2015.
DOI: 10.1007/978-3-319-19665-7_13

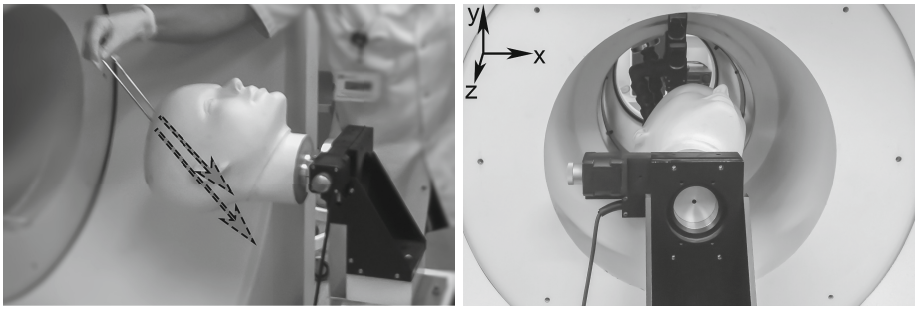


**Fig. 1.** Left: The rotating PET phantom with indication of the positions of the rods. Right: The phantom inside the Siemens HRRT scanner with the Tracoline 2.0 pointing at the face of the phantom from the far end of the bore (the dark shadow in the back).

the production line or the medical scanner. In the following the transformation, which brings the tracked motion into the coordinate system of its application will be referred to as the calibration. The required tracking accuracy and precision are often specified, while the accuracy of the calibration is overlooked. This is despite the fact that both tracking and calibration are essential for the performance of the device.

Within the field of medical brain imaging, the coordinate system of the tracking devices are calibrated to the medical scanner matching the image volume to features registered by the tracking devices. Direct point correspondence is possible if the tracking features can be identified in the image volume as for example done within magnetic resonance imaging [22] and positron emission tomography (PET) [2,14]. In these cases the tracking devices register markers that are also identified in the image volumes. Pairing image data and tracking data of the markers and optimizing a point-to-point matching the calibration transformation is obtained. With a markerless tracking device based on surface scanning the calibration can be determined directly by aligning the surface of the subject in the scanner volume [13]. In this work we quantitatively evaluate the impact of the calibration accuracy and tracking precision on image data from a Siemens High Resolution Research Tomograph (HRRT) [10]. The collected PET data are of a phantom with two line sources mounted on a rotary stage for accurate and precise angular movements. The motion of the phantom was recorded with our latest tracking prototype, Tracoline 2.0 [15]. Figure 1 shows the phantom setup in the scanner with our tracking system mounted in the far end of the narrow bore.

## 2 Method

We want to analyze the impact of inaccurate calibration and changes in precision of the tracking on motion correction applied in medical brain imaging. With an

external tracking device motion correction of scanner data is in general given as

$$\underbrace{\begin{bmatrix} x \\ y \\ z \\ 1 \end{bmatrix}}_{\text{corrected}} = \mathbf{A}_{\text{tcs2dcs}} \cdot \mathbf{A}^{-1}_{\text{corrector}}(t_0) \cdot \mathbf{A}_{\text{corrector}}(t) \cdot \mathbf{A}^{-1}_{\text{tcs2dcs}} \cdot \underbrace{\begin{bmatrix} x \\ y \\ z \\ 1 \end{bmatrix}}_{\text{uncorrected}} \tag{1}$$

where $\mathbf{A}_{\text{tcs2dcs}}$ is the result of a geometric calibration and a transformation from the tracking coordinate system (tcs) to the device coordinate system (dcs). Only for image based tracking does tcs and dcs coincide. The tracking device provides the correcting transformation $\mathbf{A}_{\text{corrector}}(t)$, which transforms the current position of the subject back to the reference position of the tracking device. To correct to a certain position in time $\mathbf{A}^{-1}_{\text{corrector}}(t_0)$ is added, allowing for correction to a given time $t_0$. The desired $t_0$ often differs from the start of the tracking device.

### 2.1 Calibration Uncertainty Simulation

In order to analyze the effect of incorrect geometric calibration, we introduce an offset in the transformation

$$\mathbf{A}_\epsilon = \begin{bmatrix} \mathbf{R}_\epsilon & \mathbf{t}_\epsilon \\ \mathbf{0} & 1 \end{bmatrix} \tag{2}$$

and apply this to the calibration transformation in (1) as follows

$$\mathbf{A}^*_{\text{tcs2dcs}} = \mathbf{A}_\epsilon \cdot \mathbf{A}_{\text{tcs2dcs}} \tag{3}$$

where the offset in translation is given by $\mathbf{t}_\epsilon = [\epsilon_x, \epsilon_y, \epsilon_z]^\top$ and offset in angles $[\epsilon_{rx}, \epsilon_{ry}, \epsilon_{rz}]$ are applied to the rotation matrix as

$$\mathbf{R}_\epsilon = \begin{bmatrix} \cos\epsilon_{rz} & -\sin\epsilon_{rz} & 0 \\ \sin\epsilon_{rz} & \cos\epsilon_{rz} & 0 \\ 0 & 0 & 1 \end{bmatrix}_{rz} \begin{bmatrix} \cos\epsilon_{ry} & 0 & \sin\epsilon_{ry} \\ 0 & 1 & 0 \\ -\sin\epsilon_{ry} & 0 & \cos\epsilon_{ry} \end{bmatrix}_{ry} \begin{bmatrix} 1 & 0 & 0 \\ 0 & \cos\epsilon_{rx} & -\sin\epsilon_{rx} \\ 0 & \sin\epsilon_{rx} & \cos\epsilon_{rx} \end{bmatrix}_{rx} \tag{4}$$

Since the calibration of a device is generally not an ongoing process, we will look at different fixed values of offset. As translation and rotation are not comparable measures, the analysis is done exclusively with offset in translation or in rotation. Such offset in calibration will result in decreasing accuracy of the applied motion correction. This inaccuracy will increase for larger motions, while no correction is applied in (1) for $\mathbf{A}_{\text{corrector}}(t) = \mathbf{I}$ as everything then factors out. The latter is regardless of calibration.

### 2.2 Tracking Precision Simulation

In order to evaluate motion correction under the effect of changes in tracking precision we apply noise to the tracking in (1)

$$\mathbf{A}_{\text{corrector}}(t)^* = \mathbf{T}^{-1}_{\text{ref}} \cdot \mathbf{A}_\epsilon(t) \cdot \mathbf{T}_{\text{ref}} \cdot \mathbf{A}_{\text{corrector}}(t) \tag{5}$$

We use $\mathbf{A}_\epsilon(t)$ as in (2) but with Gaussian noise, $\epsilon(t) = \mathcal{N}(0, \sigma^2)$. The coordinate system of the tracker can be arbitrarily chosen. Therefore, we apply the noise in a coordinate system, with origin in the mean of the tracking markers. For a markerless system, this is just the mean of the reference surface. The translation matrix $\mathbf{T}_{\text{ref}}$ moves origo to the mean of the reference. This translation can be done regardless of the device and makes the results of the analysis comparable for different devices as the translation will bring origo close to the subject in all cases. As with the analysis of geometric calibration, we analyze the effect of changes in translation and rotation separately.

### 2.3 Resolution Estimation

As a measure of performance of the motion correction of the data presented in Sec. 3, we use the full width half maximum (FWHM) of the cross section of one rod of the phantom. The rod is aligned with the principal image axes and the FWHM is measured along both axes of slices intersecting the rod. We assume the line profile of the rod cross section can be described as a Gaussian function with standard deviation $\sigma$ and mean $\mu$. The FWHM is then given as

$$\text{FWHM} = 2\sqrt{2\ln 2}\,\sigma \tag{6}$$

Errors in geometric calibration and tracking as well as the performed motion will impact the image frames of the rod in all directions. Therefore, the reported FWHM is the average along the length of the rod and also across the two dimensions of image slices intersecting the rod.

## 3 Data

A unique data set of a motion controlled PET phantom has been obtained [10]. The PET phantom was moved precisely into angular positions, while data were obtained on the Siemens HRRT scanner. The phantom consists of a low attenuation air filled mannequin head in which the positron emitting rods of Ge/Ga-68 with 3.4 MBq are inserted (Fig. 1). The left hand-side in Fig. 1 shows the orientation of the rods, which are neither parallel to each other nor to the principal image axes. The active diameter of the rods is 2.28 mm.

The mannequin head was mounted onto a rotary stage (NR360S/M, Thorlabs) with an accuracy of $0.083^o$ and a repeatability of $0.003^o$. The phantom was programmed to stay in a fixed position for 20 s at 11 angular positions between $\pm 25^o$ in steps of $5^o$.

During PET acquisition the motion of the phantom was tracked with our latest tracking prototype [15]. This system is markerless and the motion is found by continuously surface scanning the subject and registering each scan to a reference surface. The resulting angular movement of the phantom is shown in Fig. 2. Compared to the 11 different reference angular positions, we found the maximum mean error at a position to be $0.098^o$ with a standard deviation (SD)

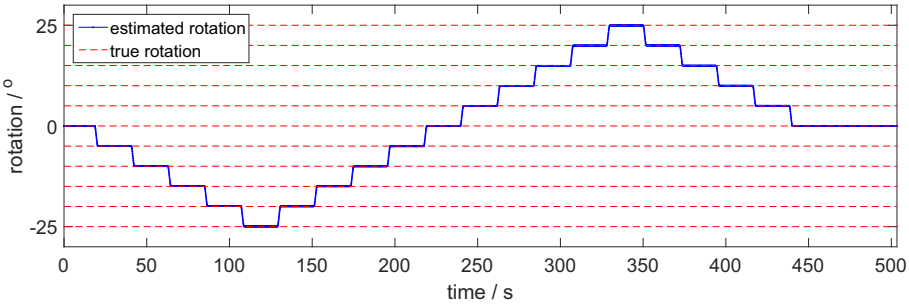


**Fig. 2.** The rotation of the rotary stage and the resulting tracking from our system. Compared to the programming of the rotary stage the tracking has an angular accuracy of $0.098^o$ and a precision of (SD) of $0.031^o$. Thorlabs reports $0.083^o$ accuracy and a repeatability of (SD) $0.003^o$ for the rotary stage (NR360S/M).

of $0.031^o$. The accuracy is very close to that of the rotary stage (difference of $0.015^o$), while the SD is a factor of 10 higher but still very small. Considering this, the tracking data can be used as a reference and by adding noise for analysis of precision. The PET data has been reconstructed using the multiple acquisition frames (MAF) method [16] with a voxelsize of 1.22 mm. The framing is based on the programmed motion of the stage. This results in 21 frames from the stationary positions (Fig. 2), while the frames with motion have been discarded. As a reference, a data set was also acquired in which the phantom remained motionless. The data sets provide a very good foundation for analysis of the impact of poor calibration and noise in tracking on motion correction. The calibration was done as an alignment between a reference surface scan from the tracking system and a point cloud extracted from a transmission volume.

## 4 Results and Discussion

The 21 PET frames with stepwise motion were repositioned according to (1) using spline interpolation. The simulated motion of the phantom is highly representative of the clinical situation, where sidewise rotations are typical. Further, the location of the rods is representative for the location of the brain. The diameter of the rod (2.28 mm) is in the order of the scanner resolution ($\sim$2 mm) across the PET field of view. Therefore the resolution of the scanner is comparable to the FWHM measured as in Sec. 2.3. The uncorrected frame with motion is shown in Fig. 3.a, while Fig. 3.d shows the corrected frame with a FWHM of 2.12 mm. The uncorrected reference with no motion is shown in Fig. 3.g and has a FWHM of 2.07 mm, which is only 0.05 mm lower than the corrected frame. This indicates a very accurate motion correction of the ruined uncorrected frame with motion.

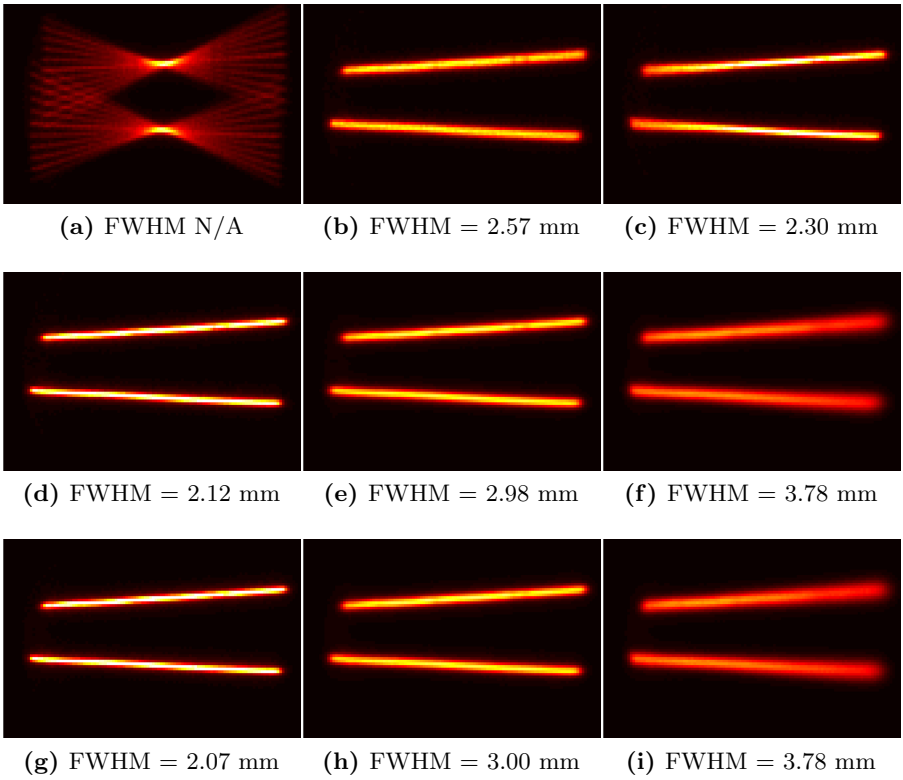

**(a)** FWHM N/A **(b)** FWHM = 2.57 mm **(c)** FWHM = 2.30 mm

**(d)** FWHM = 2.12 mm **(e)** FWHM = 2.98 mm **(f)** FWHM = 3.78 mm

**(g)** FWHM = 2.07 mm **(h)** FWHM = 3.00 mm **(i)** FWHM = 3.78 mm

**Fig. 3.** PET scans summed along the y-axis (100 mm x 140 mm region). The PET scans are corrected with different offset in the geometric calibration and noise in tracking. Uncorrected motion (a). Calibration offset: -4 mm on $y$ (b) and $4^o$ on $rx$ (c). Motion corrected (d). Tracking noise in motion correction: 1 mm SD (e) and $1^o$ SD (i). Reference with no motion (g). Reference corrected with Tracking noise: 1 mm SD (h) and $1^o$ SD (i)

### 4.1 Geometric Calibration

The motion correction was done with different offset in calibration as described in Fig. 2.1. Figure 4.a shows the measured FWHM of 3 simulations for offset of ±4 mm in the translations $\epsilon_x, \epsilon_y, \epsilon_z$. The figure shows that even for offset in the range of the voxelsize (1.22 mm) and scanner resolution (∼2 mm) there is a significant impact on the FWHM. The measured FWHM for offset in rotations $\pm 4^o$ in $\epsilon_{rx}, \epsilon_{ry}, \epsilon_{rz}$ is shown in Fig. 4.b. For offset greater than ±1 mm and $\pm 1^o$ the FWHM increases rapidly. Associated PET images for offset of 4 mm in $y$ and $-4^o$ in $rx$ are shown in Fig. 3.b and 3.c. Within the specified range in offset the FWHM grows from 2.12 to 2.57 mm for translations and 2.4 mm for rotations. The is an increase of up to 21% and considering the resulting PET images, this means that detailed brain structures cannot be distinguished to the same extent

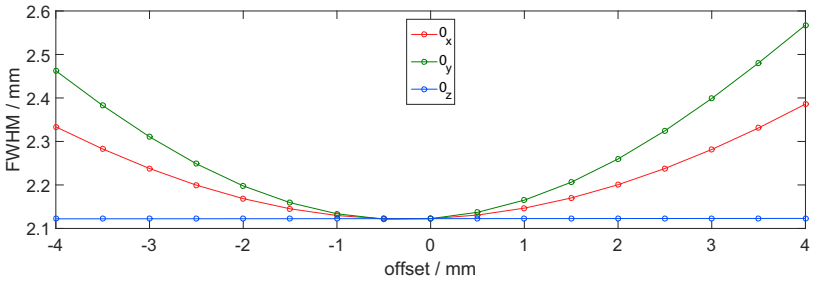


**(a)** Calibration translation offset

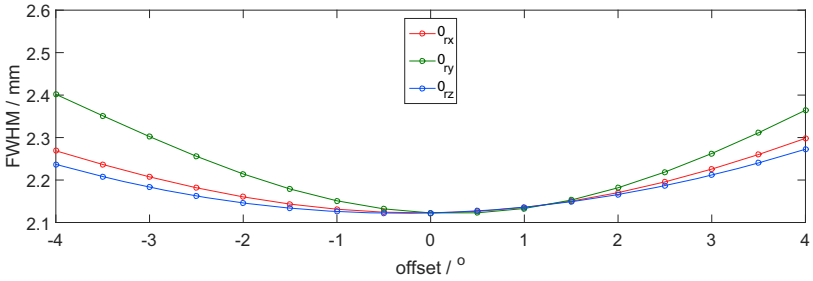


**(b)** Calibration rotation offset

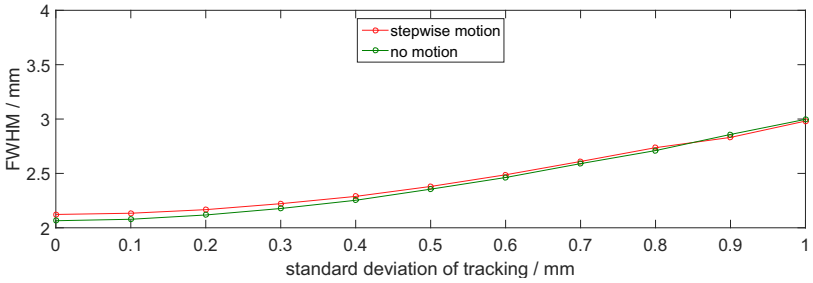


**(c)** Tracking translation noise

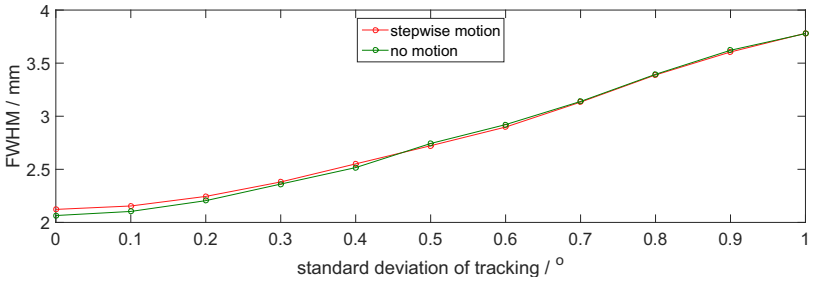


**(d)** Tracking rotation noise

**Fig. 4.** Figures (a) and (b) show the impact of offset in geometric calibration in both translation and rotation. FWHM of the active rods show great increase even for small changes in offset. Figures (c) and (d) show the impact of noise in the tracking.

and small structures such as tumors are delineated significantly larger than they are. Since the rotation of the stage is perpendicular to the $z$-axis of the scanner, offset on this axis show very little impact (Fig. 4.a). The results are correlated with the performed motion as expected. The overall results show the importance of good geometric calibration between tracking system and scanner.

### 4.2 Tracking Precision

For the analysis of tracking noise, we again motion correct the 21 PET frames, now adding noise according to Sec. 2.2. For this analysis we have added Gaussian noise to all three translations and to all three rotations separately. Since we only have 21 PET frames, we repeated the motion correction of each frame 100 times for SD of up to 1 mm for translations and 1 ($^o$) rotations. To show the degradation on a frame with no motion, we did the same for a reference scan with no motion.

Figure 4.d and 4.c show a rapidly increasing FWHM as the standard deviation grows. The path of the curves are parabolic as for the calibration simulation, however with increased amplitude especially for the rotation. The impact is similar for both the stepwise motion corrected (red) and the no motion (green). Thus applying motion correction with incorrect tracking to motionless subjects will increase the resolution. The maximal FWHM for the translation simulation is 3.00 mm at 1 mm SD (Fig. 3.e) and 3.78 mm for the rotation simulation at 1 $^o$ SD (Fig. 3.f).

## 5 Conclusion

The impact of inaccurate tracking and incorrect calibration on motion corrected PET data was investigated. The tracking precision and calibration accuracy were simulated and the resulting effect on the PET images were evaluated quantitatively. The FHWM of the PET phantom was used as an evaluation measure. This provides a measure for changes in scanner resolution.

We found that errors of the calibration had a significant impact of the FWHM even for small rotations and translations offsets in the order of the voxelsize (1.22 mm). The FWHM was increased with up to 21% from 2.12 mm to 2.57 mm for a misalignment of 4 mm.

The impact of the tracking precision was even more important. The FWHM increased with 78% to 3.78 mm when adding noise to the rotation of the tracking with SD of 1$^o$. The simulated errors of the calibration and the tracking are not directly comparable. However, variation in precision of the tracking in the tenths of a millimeter/degree has similar impact on the resolution as calibration errors in the millimeters/degrees range.

The results show a significant improvement on the frame with motion even with offset in calibration and noise in tracking, while the reference is heavily degraded. This indicates that there is a threshold for the benefit of motion correction, which is a relation between the quality of the tracking system and the amount of motion.

## References


1. Aksoy, M., Forman, C., Straka, M., Skare, S., Holdsworth, S., Hornegger, J., Bammer, R.: Real-time optical motion correction for diffusion tensor imaging. Magnetic Resonance in Medicine **66**(2), 366–378 (2011)
2. Bühler, P., Just, U., Will, E., Kotzerke, J., van den Hoff, J.: An accurate method for correction of head movement in PET. IEEE Transactions on Medical Imaging **23**, 1176–1185 (2004)
3. Cai, Q., Aggarwal, J.K.: Tracking human motion using multiple cameras. Proceedings of the 13th International Pattern Recognition **3**, 68–72 (1996)
4. Chaumette, F., Rives, P., Espiau, B.: Positioning of a robot with respect to an object, tracking it and estimating its velocity by visual servoing. In: Proceedings of the 1991 IEEE International Conference on Robotics and Automation, 1991, pp. 2248–2253. IEEE (1991)
5. Darrow, R.D., Dumoulin, C.L., Souza, S.P.: Tracking system to monitor the position and orientation of a device using multiplexed magnetic resonance detection, US Patent 5,318,025, June 7, 1994
6. Fried, M.P., Kleefield, J., Gopal, H., Reardon, E., Ho, B.T., Kuhn, F.A.: Image-guided endoscopic surgery: Results of accuracy and performance in a multicenter clinical study using an electromagnetic tracking system. The Laryngoscope **107**(5), 594–601 (1997)
7. Fulton, R., Meikle, S., Eberl, S., Pfeiffer, J., Constable, C., Fulham, M.: Correction for head movements in positron emission tomography using an optical motion-tracking system. IEEE Transactions on Nuclear Science **49**, 116–123 (2002)
8. Geng, Z.: Method and system for three-dimensional imaging using light pattern having multiple sub-patterns US Patent 6,700,669, Mar 2, 2004
9. Horton, M., Newton, A.: Method and apparatus for determining position and orientation of a moveable object using accelerometers. US Patent 5,615,132, Mar 25, 1997
10. Jensen, R.R., Olesen, O.V., Benjaminsen, C., Højgaard, L., Larsen, R.: Markerless PET motion correction: tracking in narrow gantries through optical fibers. In: IEEE Nuclear Science Symposium Conference Record, pp. M10–M24 (2014)
11. Lopresti, B.J., Russo, A., Jones, W.F., Fisher, T., Crouch, D.G., Altenburger, D.E., Townsend, D.W.: Implementation and performance of an optical motion tracking system for high resolution brain PET imaging. IEEE Transactions on Nuclear Science **46**(6), 2059–2067 (1999)
12. Maclaren, J., Armstrong, B.S., Barrows, R.T., Danishad, K., Ernst, T., Foster, C.L., Gumus, K., Herbst, M., Kadashevich, I.Y., Kusik, T.P., et al.: Measurement and correction of microscopic head motion during magnetic resonance imaging of the brain. PLOS one **7**(11), e48088 (2012)
13. Olesen, O.V., Sullvian, J.M., Morris, E.D., Mulnix, T., Paulsen, R.R., Højgaard, L., Roed, B., Larsen, R.: List-mode PET motion correction using markerless head tracking: proof-of-concept in human studies. IEEE Transactions on Medical Imaging **32**, 200–209 (2013)
14. Olesen, O.V., Svarer, C., Sibomana, M., Keller, S., Holm, S., Jensen, J., Andersen, F., Højgaard, L.: A movable phantom design for quantitative evaluation of motion correction studies on high resolution PET scanners. IEEE Transactions on Nuclear Science **57**(3), 1116–1124 (2010)
15. Olesen, O.V., Wilm, J., van der Kouwe, A., Jensen, R.R., Larsen, R., Wald, L.L.: An MRI compatible surface scanner. In: Joint Annual Meeting ISMRM-ESMRMB and SMRT 23rd Annual Meeting Conference Record, p. 1303 (2014)

16. Picard, Y., Thompson, C.J.: Motion correction of PET images using multiple acquisition frames. IEEE Transactions on Medical Imaging **16**(2), 137–144 (1997)
17. Qin, L., van Gelderen, P., Derbyshire, J.A., Jin, F., Lee, J., de Zwart, J.A., Tao, Y., Duyn, J.H.: Prospective head-movement correction for high-resolution mri using an in-bore optical tracking system. Magnetic Resonance in Medicine **62**(4), 924–934 (2009)
18. Raab, F.H., Blood, E.B., Steiner, T.O., Jones, H.R.: Magnetic position and orientation tracking system. IEEE Transactions on Aerospace and Electronic Systems **5**(5), 709–718 (1979)
19. Schulz, J., Siegert, T., Reimer, E., Labadie, C., Maclaren, J., Herbst, M., Zaitsev, M., Turner, R.: An embedded optical tracking system for motion-corrected magnetic resonance imaging at 7T. Magnetic Resonance Materials in Physics, Biology and Medicine **25**(6), 443–453 (2012)
20. Seiler, P., Blattmann, H., Kirsch, S., Muench, R., Schilling, C.: A novel tracking technique for the continuous precise measurement of tumour positions in conformal radiotherapy. Physics in medicine and biology **45**(9), N103 (2000)
21. Watzinger, F., Birkfellner, W., Wanschitz, F., Millesi, W., Schopper, C., Sinko, K., Huber, K., Bergmann, H., Ewers, R.: Positioning of dental implants using computer-aided navigation and an optical tracking system: case report and presentation of a new method. Journal of Cranio-Maxillofacial Surgery **27**(2), 77–81 (1999)
22. Zaitsev, M., Dold, C., Sakas, G., Hennig, J., Speck, O.: Magnetic resonance imaging of freely moving objects: prospective real-time motion correction using an external optical motion tracking system. Neuroimage **31**(3), 1038–1050 (2006)